Research Article | Vol. 8, No. 10 | 1 Oct 2017 | BIOMEDICAL OPTICS EXPRESS 4663
Biomedical Optics EXPRESS

Characterization of the mechanical properties of resected porcine organ tissue using optical fiber photoelastic polarimetry

ALEXA W. HUDNUT,[1] BEHZAD BABAEI,[2] SONYA LIU,[3] BRENT K. LARSON,[4] SHANNON M. MUMENTHALER,[3] AND ANDREA M. ARMANI[1,*]

[1]*Department of Biomedical Engineering, University of Southern California, Los Angeles, CA, 90089, USA*
[2]*Neuroscience Research Australia, Randwick, Australia*
[3]*Lawrence J. Ellison Institute for Transformative Medicine, University of Southern California, Los Angeles, CA, 90033, USA*
[4]*Department of Pathology and Laboratory Medicine, Cedars-Sinai Medical Center, Los Angeles, CA, 90048, USA*
[*]*armani@usc.edu*

Abstract Characterizing the mechanical behavior of living tissue presents an interesting challenge because the elasticity varies by eight orders of magnitude, from 50Pa to 5GPa. In the present work, a non-destructive optical fiber photoelastic polarimetry system is used to analyze the mechanical properties of resected samples from porcine liver, kidney, and pancreas. Using a quasi-linear viscoelastic fit, the elastic modulus values of the different organ systems are determined. They are in agreement with previous work. In addition, a histological assessment of compressed and uncompressed tissues confirms that the tissue is not damaged during testing.

OCIS codes: (120.5410) Polarimetry; (120.3890) Medical optics instrumentation; (120.4290) Nondestructive testing.

References and links

1. J. Rosen, J. D. Brown, S. De, M. Sinanan, and B. Hannaford, "Biomechanical Properties of Abdominal Organs In Vivo and Postmortem Under Compression Loads," J. Biomech. Eng. **130**, 021020 (2008).
2. D. C. Stewart, A. Rubiano, M. M. Santisteban, V. Shenoy, Y. Qi, C. J. Pepine, M. K. Raizada, and C. S. Simmons, "Hypertension-linked mechanical changes of rat gut," Acta Biomater. **45**, 296–302 (2016).
3. A. Calzado-Martín, M. Encinar, J. Tamayo, M. Calleja, and A. San Paulo, "Effect of Actin Organization on the Stiffness of Living Breast Cancer Cells Revealed by Peak-Force Modulation Atomic Force Microscopy," ACS Nano **10**(3), 3365–3374 (2016).
4. S. E. Cross, Y. S. Jin, J. Rao, and J. K. Gimzewski, "Nanomechanical analysis of cells from cancer patients," Nat. Nanotechnol. **2**(12), 780–783 (2007).
5. M. E. Grady, R. J. Composto, and D. M. Eckmann, "Cell elasticity with altered cytoskeletal architectures across multiple cell types," J. Mech. Behav. Biomed. Mater. **61**, 197–207 (2016).
6. K. J. Parker, M. M. Doyley, and D. J. Rubens, "Imaging the elastic properties of tissue: the 20 year perspective," Phys. Med. Biol. **56**(1), R1–R29 (2011).
7. E. A. Corbin, O. O. Adeniba, R. H. Ewoldt, and R. Bashir, "Dynamic mechanical measurement of the viscoelasticity of single adherent cells," Appl. Phys. Lett. **108**(9), 093701 (2016).
8. W. J. Eldridge, Z. A. Steelman, B. Loomis, and A. Wax, "Optical Phase Measurements of Disorder Strength Link Microstructure to Cell Stiffness," Biophys. J. **112**(4), 692–702 (2017).
9. D. Qi, N. Kaur Gill, C. Santiskulvong, J. Sifuentes, O. Dorigo, J. Rao, B. Taylor-Harding, W. Ruprecht Wiedemeyer, and A. C. Rowat, "Screening cell mechanotype by parallel microfiltration," Sci. Rep. **5**(1), 17595 (2015).
10. H. K. Hunt and A. M. Armani, "Label-free biological and chemical sensors," Nanoscale **2**(9), 1544–1559 (2010).
11. T. H. Chua and C.-L. Chen, "Fiber polarimetric stress sensors," Appl. Opt. **28**(15), 3158–3165 (1989).
12. A. Barlow and D. Payne, "The stress-optic effect in optical fibers," IEEE J. Quantum Electron. **19**(5), 834–839 (1983).
13. A. W. Hudnut and A. M. Armani, "High-resolution analysis of the mechanical behavior of tissue," Appl. Phys. Lett. **110**(24), 243701 (2017).
14. M. C. Harrison and A. M. Armani, "Portable polarimetric fiber stress sensor system for visco-elastic and biomimetic material analysis," Appl. Phys. Lett. **106**(19), 191105 (2015).
15. Y.-c. Fung, *Biomechanics: Mechanical Properties of Living Tissues* (Springer Science & Business Media, 1981).

#304145 https://doi.org/10.1364/BOE.8.004663
Journal © 2017 Received 7 Aug 2017; revised 14 Sep 2017; accepted 15 Sep 2017; published 25 Sep 2017

Biomedical Optics EXPRESS

16. B. Babaei, S. D. Abramowitch, E. L. Elson, S. Thomopoulos, and G. M. Genin, "A discrete spectral analysis for determining quasi-linear viscoelastic properties of biological materials," J. R. Soc. Interface **12**(113), 20150707 (2015).
17. S. Thomopoulos, G. R. Williams, J. A. Gimbel, M. Favata, and L. J. Soslowsky, "Variation of biomechanical, structural, and compositional properties along the tendon to bone insertion site," J. Orthop. Res. **21**(3), 413–419 (2003).
18. S. Goenezen, J. F. Dord, Z. Sink, P. E. Barbone, J. Jiang, T. J. Hall, and A. A. Oberai, "Linear and Nonlinear Elastic Modulus Imaging: An Application to Breast Cancer Diagnosis," IEEE Trans. Med. Imaging **31**(8), 1628–1637 (2012).
19. D. Kasper, A. Fauci, S. Hauser, D. Longo, and J. Jameson, *Harrison's Principles of Internal Medicine* (McGraw-Hill Education, 2015).
20. M. Perepelyuk, L. Chin, X. Cao, A. van Oosten, V. B. Shenoy, P. A. Janmey, and R. G. Wells, "Normal and Fibrotic Rat Livers Demonstrate Shear Strain Softening and Compression Stiffening: A Model for Soft Tissue Mechanics," PLoS One **11**(1), e0146588 (2016).
21. C. Chui, E. Kobayashi, X. Chen, T. Hisada, and I. Sakuma, "Transversely isotropic properties of porcine liver tissue: experiments and constitutive modelling," Med. Biol. Eng. Comput. **45**(1), 99–106 (2007).
22. K. Arda, N. Ciledag, E. Aktas, B. K. Aribas, and K. Köse, "Quantitative Assessment of Normal Soft-Tissue Elasticity Using Shear-Wave Ultrasound Elastography," AJR Am. J. Roentgenol. **197**(3), 532–536 (2011).
23. J. M. Mattice, A. G. Lau, M. L. Oyen, and R. W. Kent, "Spherical indentation load-relaxation of soft biological tissues," J. Mater. Res. **21**(08), 2003–2010 (2006).
24. S. Nasseri, L. E. Bilston, and N. Phan-Thien, "Viscoelastic properties of pig kidney in shear, experimental results and modelling," Rheol. Acta **41**(1-2), 180–192 (2002).
25. A. Anssari-Benam, D. L. Bader, and H. R. C. Screen, "A combined experimental and modelling approach to aortic valve viscoelasticity in tensile deformation," J. Mater. Sci. Mater. Med. **22**(2), 253–262 (2011).
26. J. Vincent, *Structural Biomaterials Third Edition* (Princeton University Press, 2012).

1. Introduction

Compressive testing is one of the most robust methods for measuring the mechanical properties of tissues due to the large range in Young's Modulus values, from 50Pa-5GPa [1,2]. However, current techniques either suffer from poor spatial resolution or require destructive sample processing. For example, the large sensor area in rheology systems results in a poor spatial resolution, on the order of centimeters. To address this, researchers turned to Atomic Force Microscopy (AFM) [3–5]. However, destructive sample preparation is required, preventing further imaging and molecular analysis. Given these issues, researchers have begun to develop alternative approaches. Several elastography methods have been developed in an attempt to bridge these traditional techniques, including ultrasound elastography, magnetic resonance elastography, and optical coherence elastography [6]. However, there remain issues with resolution and understanding tissues with micron-scale heterogeneity. Parallel efforts have emphasized single cell methods, leaving tissue-level analysis out of reach [7–9].

Optics is a robust platform for bio/chemical sensors because devices can be constructed with small and adjustable sensing regions. Previous work has focused on refractometric approaches where the signal is generated when a molecule directly disturbs the optical field [10]. Recently, optical fiber sensor research has expanded from evanescent field detection to include approaches based on the photo-elastic (PE) effect [11, 12]. In PE sensors, the optical field does not directly interact with the sample. Therefore, the transmitted power is more stable and the sensor is less susceptible to degradation. A variant of PE detection is PE-induced polarization detection. In this approach, the change in the refractive index induces a change in the polarization state of the optical field. Because this approach is less susceptible to noise, it offers an improvement in overall detection sensitivity while maintaining the other advantages of a PE detection method. For example, in previous work, an optical fiber polarimetric elastography instrument demonstrated the ability to detect sub-mm collagen membranes embedded in mm-thick slices of salmon muscle [13]. However, a key milestone in the development of this system is the non-destructive characterization of freshly excised tissues in the delay phase before rigor mortis. This achievement has yet to be shown.

In the present work, optical fiber photoelastic polarimetry (PEP) is used to analyze the material properties of freshly excised porcine liver, kidney, and pancreas tissue before the

Biomedical Optics EXPRESS

onset of rigor mortis. Histological analyses demonstrate that the tissue is undamaged at the microscale after compressive testing. A Quasi-linear viscoelasticity (QLV) model is used to analyze and fit the experimental data, providing a rigorous approach for analyzing the organ mechanical properties. Notably, this study demonstrates that the PEP method is able to maintain high resolution of mechanical behavior analysis in core biopsy samples without *a priori* damaging sample preparation.

2. Materials and methods

2.1. Optical fiber photoelastic polarimetry (PEP)

The detection system combines conventional compressive testing with an optical fiber PEP sensor. The sensor is located under the tissue sample, and compression is applied vertically via a motorized plunger (Fig. 1). A 1.5mW 1550nm laser is connected to an in-line fiber polarizer before the light enters a section of polarization maintaining (PM) optical fiber, which runs under the 7mm x 7mm x 4mm sample to create the sensor. The diameter of the optical fiber sensor is 250μm, and the optical mode field diameter, which is the reactive region of the fiber, is 6.6 μm. A polarimeter is connected to the output of the fiber to detect the polarization state, which is recorded on a laptop.

The duration of the loading-unloading interval is 30 seconds (15 seconds loading and 15 seconds unloading), and data is taken every 30ms for a total of 1024 data points. The three Stokes parameters are used to determine the change in polarization state (ΔPol) due to compression [11, 14]. The ΔPol is directly proportional to the stress within the sample. The instrument is reconfigured each day, and the PM optical fiber sensor is replaced. For each sample, three strains (10%, 20%, and 30%) are applied for the measurements. Each strain is tested five times, and N>75 samples are tested to ensure reproducibility of the results. Additional details can be found in previously published works [11, 14].

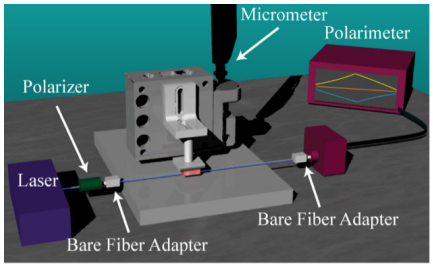

Fig. 1. Rendering of the testing setup demonstrating the position of the sample, optical fiber and compressive stage.

2.2. Histological analysis

Matched pairs of compressed and uncompressed samples from each organ are fixed in 10% neutral buffered formalin for 24 hr, paraffin-embedded, and sectioned at 5μm thickness. Hematoxylin and eosin (H&E) stains are performed according the manufacturer's instructions (Leica Biosystems). All of the tissues from a given organ are prepared together.

2.3. Quasi-linear viscoelasticity theory

The predominant method for fitting loading-unloading curves within the biomaterials community is the Quasi-Linear Viscoelasticity (QLV) method [15–17]. This method provides material constants that can directly be compared between samples and measurements [16].

The QLV uses the relaxation function (G(t)) and the elastic stress response $\sigma^e(\varepsilon)$ to determine the stress at a specific time and strain [15]:

Biomedical Optics EXPRESS

$$\sigma(\varepsilon,t)=\int_{-\infty}^{t}G(t-u)\frac{\delta\sigma^{e}}{\delta\varepsilon}\frac{\delta\varepsilon}{\delta u}du \tag{1}$$

where σ is the stress measured by the polarimeter (ΔPol), ε is the strain and u is a dummy index. The relaxation function is:

$$G(t)=\frac{1+\int_{\tau_1}^{\tau_2}\left(Ce^{-t/\tau}/\tau\right)d\tau}{1+\int_{\tau_1}^{\tau_2}\left(C/\tau\right)d\tau} \tag{2}$$

where C is the damping coefficient, and τ_1 and τ_2 represent the upper and lower boundary of the time constants of relaxation.

The elastic stress response is $\sigma^{e}(\varepsilon)=A\left(e^{B\varepsilon}-1\right)$, where A is the elasticity parameter and B is the non-linearity parameter. Specifically, B describes the exponential increase in stiffness with increasing strain, which is due in part to the collagen makeup and cellular plasticity [18].

2.4. Preparation of porcine samples

Twelve pigs were used for testing. A section of tissue, approximately 10cm x 5cm x 5cm, was excised from each of the three organs, and tested within two hours. The pigs were alive and under anesthesia during resection. The samples were placed in RPMI on ice until testing. The studies were conducted under Department of Animal Resource Tissue Request Form 10843.

3. Results

3.1. Histology results

Figure 2 shows representative H&E images from tissues compressively tested with the optical fiber PEP device. Hematoxylin (blue/purple) stains acidic components of the tissues (DNA), and eosin (pink) stains basic components of the tissues (ECM). The H&E stain can be used to indicate the damage to microstructures within the tissue, and if the individual cells and nuclei remain intact. A cursory inspection of Fig. 2 indicates that the nuclei and cellular borders remain intact and distinct in all tissue types, verifying that the compressive testing has minimal impact on the cellular structure.

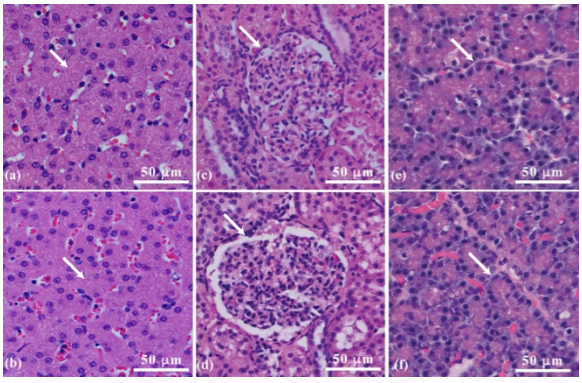

Fig. 2. Histology images from each of the three organs: (a) uncompressed and (b) compressed liver sample, (c) uncompressed and (d) compressed kidney sample, (e) uncompressed and (f) compressed pancreas sample. The arrows indicate microstructures of interest.

For the liver (Fig. 2(a) and 2(b)), hepatocytes are used to identify whether damage occurs. Hepatocytes are the primary component of the liver, making up more than 70% of liver cells. They synthesize proteins and filter exogenous and endogenous compounds within the liver

Biomedical Optics EXPRESS

[19]. By comparing the uncompressed (Fig. 2(a)) to the compressed liver tissue (Fig. 2(b)), it is clear that the hepatocytes remain intact, confirming that testing does not impact the tissue structure. Though not shown, the portal triads and the central veins remained intact.

For the kidney (Fig. 2(c) and 2(d)), the glomerulus is used to identify whether damage occurs due to its complex structure and distinct characteristics. The glomerulus is a network of capillaries in the kidney where the blood is filtered [19]. By comparing the structure of the glomerulus in the images of the uncompressed (Fig. 2(c)) and the compressed (Fig. 2(d)) kidney tissue, it is clear that the glomerulus is not affected by testing. The nuclei are intact and red blood cells are intraluminal, indicating capillary walls remain intact. Though not depicted in Fig. 2, the proximal and distal tubules also remained intact.

For the pancreas (Fig. 2(e) and 2(f)), the acinar cells are used to identify whether damage occurs to the tissue. The acinar cells are exocrine cells within the pancreas, which produce enzymes [19]. Due to their unique structure and enzymatic load, they are selected as the marker of damage. By comparing the structure of the acinar cells in the images of the uncompressed (Fig. 2(e)) and the compressed (Fig. 2(f)) pancreas tissue, it is clear that the acinar cells are not affected. Though not depicted in Fig. 2, the ducts and islets remained intact with crisp nuclei and clear cellular borders.

3.2. Optical fiber PEP results

The loading-unloading curves for each organ at 10%, 20%, and 30% strain are shown in Fig. 3. Each loading-unloading curve is normalized to start at (0,0). Therefore, for all samples, there is a negative final ΔPol value for each unloading curve. This indicates that there is residual strain within the sample between susbsequent runs. The accumulation of residual strain signifies that there is irreversible compression of the tissue.

The liver exhibits a very linear response, at 10% strain in the loading-unloading curves, indicating an elastic response (Fig. 3(a)). Of the three organs tested, the liver had the most consistent and linear response at this strain. As the strain increases, the liver begins to exhibit some viscoelastic behavior as indicated by hysteresis in the loading-unloading curves. The results for the kidney and the pancreas show definitively different behavior than the liver at 10% strain (Fig. 3(b) and 3(c)). Both exhibit viscoelastic behavior, even at 10% strain.

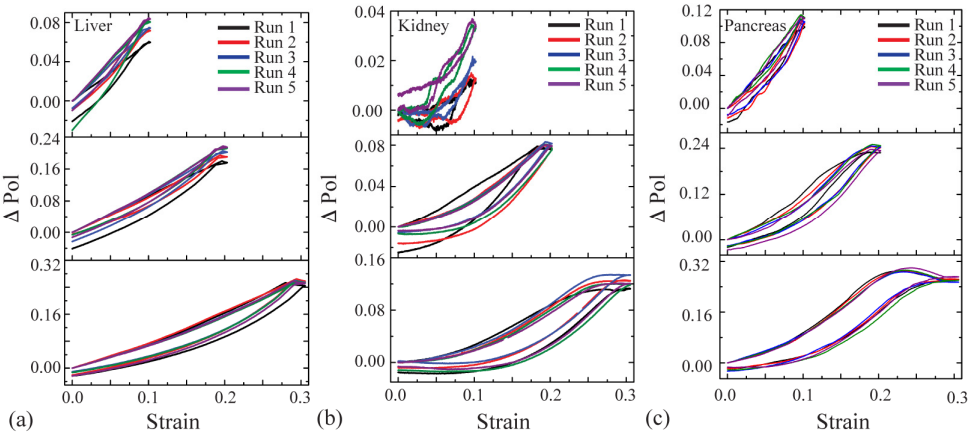

Fig. 3. (a) Loading-unloading curves from a liver sample. (b) Loading-unloading curves from a kidney sample. (c) Loading-unloading curves from a pancreas sample.

The relative change in polarization (ΔPol) increases linearly as the strain increases. The maximum ΔPol values provide a baseline for understanding the relative stiffness of the tissue. One would expect the total ΔPol to increase from liver to kidney to pancreas. However, because the device is reconfigured and the optical fiber is replaced each day, the alignment of

Biomedical Optics EXPRESS

the fast and slow axis of the PM fiber sensor rotates, changing the sensor response. Another consequence of this variable alignment is that the kidney results at 10% strain appear more noisy than the other two organs. This indicates the alignment of the optical fiber was closer to the limit of detection when the kidney was tested. This effect motivated the use of the QLV fit method to determine the elasticity values.

The non-linearity of the mechanical behavior increases as the strain increases. In the kidney at 30% strain, there is a flattening of the curve at the end of the compression, indicating the reversible rearrangement of internal microstructures (Fig. 3(b)). In the pancreas at 30% strain, the flattening of the curve is even more pronounced (Fig. 3(c)). This response is likely due to the unique microstructure within the pancreas. The precise structure that could give rise to this behavior is actively under investigation.

3.3. QLV fitting results

To determine the material coefficients for different organs, we fit our experimental data for strain and ΔPol (α stress) in Matlab to the QLV model. The result is a numerical solution for each of the five coefficients: A, B, C, τ_1, and τ_2. Example data sets and associated QLV model fits are presented in Fig. 4 for each organ. The QLV model is able to accurately fit each of the three organs, although it has some difficulty fitting the flattening at the end of the high strain curves for the kidney and pancreas. The QLV fit is applied to each loading-unloading curve, so that the results can be compared within data sets from the same organ and across data sets from different organs. Comparing the fit of the data across different organs is an example of using the fit to correlate data sets with variable device configuration. This is because each of the organs is tested on a different day and the optical fiber alignment is slightly changed every time the disposable fiber sensor is replaced.

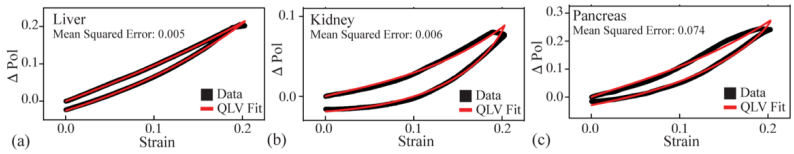

Fig. 4. Plot of data from a single loading-unloading curve for (a) liver, (b) kidney, and (c) pancreas with the corresponding QLV fit. The data and fit are from Run 2 at 20% strain.

The coefficients determined from the QLV fit of the experimental data, and energy loss are plotted in Fig. 5. The elastic modulus of the material is represented by coefficient A (Fig. 5(a)). Because it is determined from the fit of the loading-unloading curve, coefficient A is independent of the device configuration. Therefore, it can be used to compare multiple organs across different days of testing. The general trend in the measurements is as the strain increases the elastic modulus increases. This behavior is commonly observed in viscoelastic materials [2, 20]. The experimentally determined range of elastic modulus values using the optical fiber PEP method and QLV fit is 0.1-0.5 KPa for liver, 0.15-0.9 KPa for kidney, and 0.2-8.0 KPa for pancreas. Our results are within the range of previously published elastic modulus values [1, 2, 20–24]. Previously reported elastic modulus values vary due to several factors, including the animal model, sample preparation method, and mathematical fit used. Therefore, we determine the QLV fit provides a realistic value for the elastic modulus.

Biomedical Optics EXPRESS

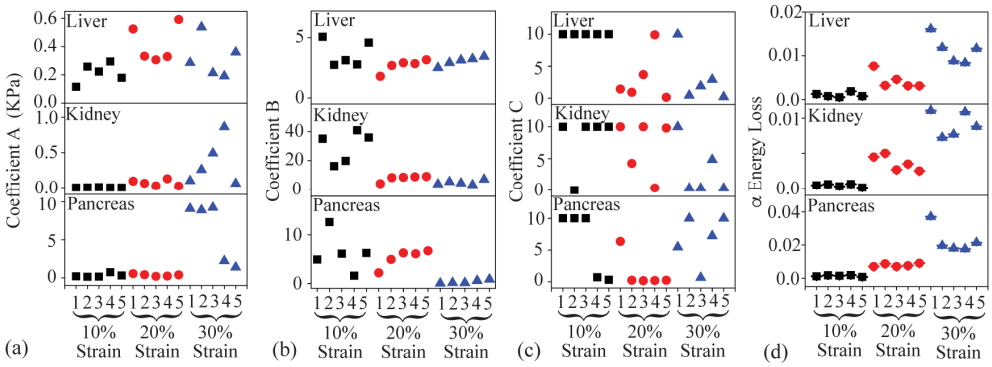

Fig. 5. Summary of (a) coefficient A- elasticity parameter, (b) coefficient B - non-linearity parameter, (c) coefficient C - damping coefficient, and (d) energy loss.

Coefficient B represents the non-linearity within the system (Fig. 5(b)). This has several contributing factors including the ECM composition and cellular plasticity. The general trend in the measurements is that as the strain increases, the non-linearity decreases. This response is due to the fact that as the rate of compression increases, the impact of the different non-linear components decreases. The amount that B changes with strain in liver and pancreas is significantly less than in kidney. This is because the kidney's micro-architecture and cellular diversity is significantly more complex than either the liver or the pancreas [19].

Coefficient C represents the damping coefficient of the material (Fig. 5(c)). The damping coefficient is an intrinsic material property that indicates whether a material will return energy to a system. It has previously been used to determine the amount of mechanical energy dissipated in biomaterials [25]. The damping coefficient helps elucidate the impact of multiple runs on the mechanical properties of the tissues. While the QLV fit can provide information about the energy dissipated within the sample, the values decrease in accuracy as strain increases. This is in part due to the poor fit of the model at the extremes of the data.

Energy loss represents the irreversible compression and destruction of microarchitectures of the material due to repeated compression (Fig. 5(d)) [26]. To determine a value proportional to the energy loss, the area between the loading-unloading curves is calculated. The general trend in the measurements is the energy loss decreases with consecutive compressions at high strain, indicating the samples may undergo physical changes as a result of the compression. While these results appear to contradict the H&E images in Fig. 2, it is important to realize that the histology focused on microscale defects. There are several hypotheses for the precise mechanism of energy dissipation, which are currently under further investigation.

4. Conclusions

Using the portable optical fiber PEP instrument in combination with a QLV model, the mechanical properties of three different porcine organs are successfully measured. The values for the elastic modulus agree with previously published work. Using histology, it is determined that the method does not damage the tissue. This work sets the stage for future research studying the time-dependent properties of living tissue as well as correlating microscale architecture with molecular and cellular features. Additionally, based on these same fundamental properties, future work in the device arena will include developing smaller, integrated versions of this instrument for in situ testing.

Funding

Office of Naval Research [N00014-11-1-0910, N00014-17-2270], A. E. Mann Graduate Research Fellowship, and the Zumberge Research Fund.

Biomedical Optics EXPRESS

Acknowledgements

R.A. Arboleda, C. Arnesano, G. Genin, M. Harrison, N. Katkhouda, and Q.Wang.

Disclosures

The authors declare that there are no conflicts of interest related to this article.